Inelastic proton scattering from Pt isotopes and the interacting boson model

A. Sethi, N. M. Hintz, D. N. Mihailidis, A. M. Mack, and M. Gazzaly
School of Physics, University of Minnesota, Minneapolis, Minnesota 55455

K. W. Jones
Los Alamos National Laboratory, Los Alamos, New Mexico 87545

G. Pauletta and L. Santi
University of Udine, Udine, UD-33100, Italy

D. Goutte
Centre d'Etudes Nucléaires de Saclay, F-91191, Gif-sur-Yvette, France
(Received 6 May 1991)

Inelastic proton scattering has been used to measure the $d\sigma/d\Omega$ and A_y angular distributions for several low-lying collective states in ^{194,196}Pt using 647 MeV polarized protons with special emphasis on the excitation of the 4^+ states below 2 MeV. The data have been analyzed in the framework of the coupled-channels scheme using the program ECIS. Large $E4$ transition strengths to the 4^+ states in both nuclei are found in sharp contrast with the predictions of the interacting boson model with only s ($L=0$) and d ($L=2$) bosons. It is found that although the $E2$ properties of these nuclei are consistent with the interacting boson model (sd) predictions, higher degrees of freedom, e.g., g ($L=4$) bosons, need to be invoked in order to get a reasonable agreement with the measured $E4$ properties.

I. INTRODUCTION

Platinum isotopes belong to a very interesting but complex region of the periodic table known as the transition region. These nuclei are characterized by shape changes between spherical and deformed. The transition region can be grouped into two parts: the light transitional nuclei; e.g., Nd, Sm, and Gd undergo a rather sudden change in shape from spherical to prolate axially symmetric deformed with the deformation setting in around $N\sim 90$. The heavy transitional nuclei (W, Os, Pt, and Hg), in contrast, exhibit a gradual change from a prolate shape [static quadrupole moment, $Q(2_1^+)<0$] for the Os isotopes [1–3] to an oblate shape [$Q(2_1^+)>0$] for the Pt isotopes [4–8]. The prolate-oblate transition sets in around $A\sim 192$. Because of the complex and diverse nature of these transitions, simple rotational and/or vibrational models have proven to be inadequate for these nuclei. Various models have been used to study these nuclei in the past, e.g., the rigid asymmetric rotor model (ARM) [9,10], rotation-vibration models (RVM's) with symmetric [11] and asymmetric [12] shape, and the γ-unstable model [13]. Extensions of these models have also been invoked, such as the ARM with a variable moment of inertia [14] and a β_4 deformation [15], and the generalized collective model (GCM) [16] which assumes an arbitrary-shape potential-energy surface. In addition, there have been microscopic [17] and semimicroscopic [18] calculations and more recent results from the boson expansion theory of Weeks and Tamura [19]. All of these models have had mixed success in the transition region.

With the emergence of the interacting boson model (IBM) [20], however, it has become possible to give a simple and consistent description of the transition region. In its simple form, known as IBM-1, the model describes the low-lying collective excitations of an even-even nucleus in terms of the s ($L=0$) and d ($L=2$) bosons. A comprehensive review of the model and its application to the transition region has been recently given by Casten and Warner [21]. As the s and d bosons span a six-dimensional Hilbert space, the Hamiltonian corresponding to the IBM-1 has a group structure U(6). The three limiting symmetries of this Hamiltonian, SU(5), SU(3), and O(6), correspond to the geometrical shapes, spherical vibrator, symmetric rotor, and γ-unstable rotor, respectively. In fact, ^{196}Pt is considered to be a very good example of the O(6) limit [22,23]. Therefore, the Pt→Os transition can be treated in terms of small departures from the O(6) limit of the IBM to the SU(3) limit [24]. The model has been remarkably successful in reproducing a large body of $E2$ data consisting of level schemes and transition rates across the Pt-Os region [24]. However, the same model scheme has been found incapable of giving a reasonable description of the $E4$ data [25,26], in particular the transition rates from the ground state to the low-lying 4^+ states. We argue that, for the high-spin states, the simple assumptions of the IBM model (s and d bosons) are too restrictive and that one needs to include higher degrees of freedom, e.g., g ($L=4$) boson in the IBM. In this paper we investigate this extension of the model to describe the low-lying 4^+ states in the two platinum isotopes ^{194,196}Pt.

In the past ^{194,196}Pt have been studied with a wide variety of probes. Among the earliest of these studies were the Coulomb excitation experiments done by the

Pittsburgh group [4–7]. The focus of this work was the precision measurement of the $E2$ transition probability and the quadrupole moment of the first excited state to investigate the prolate-oblate transition in the Os-Pt region. Recently, Gyapong *et al.* [8] have performed similar experiments using α particles, ^{12}C and ^{16}O on $^{194,196,198}Pt$ as a test of the Pittsburgh measurements. There have been other Coulomb excitation experiments [26–32] as well aimed at studying the level structure and the $B(E2)$'s in these nuclei. In some of these, levels as high as $J^{\pi}=10^{+}$ have been excited using heavy ions. Information on the Pt isotopes has also come from studies of β-decay [33–36], deuteron breakup $(d,pn\gamma)$ [37], two-nucleon transfer (p,t) [38], and average resonance neutron capture (n,γ) [23] experiments. In Ref. [23], quite detailed information on the level structure and branching ratios of low-spin states in ^{196}Pt was given.

In an effort to study the higher multipole moments, inelastic-scattering experiments with electrons [39], protons [26,40], α particles [41], and ^{12}C ions [42] have also been performed. $J^{\pi}=4^{+}$ states in $^{194,196}Pt$ have been previously studied with proton [26] and electron [39] scattering, respectively. Because of the competing contributions of one-step and multistep channels, proton scattering is an excellent means of determining the higher multipole moments. The aim of the present experiment was the precision measurement of the $E4$ moments for the low-lying 4^{+} states below 2 MeV in $^{194,196}Pt$ and a comparison with the predictions of the IBM.

II. EXPERIMENT

The experiment was performed using the High-Resolution Spectrometer (HRS) at the Clinton P. Anderson Meson Facility of the Los Alamos National Laboratory (LANL). Details of the detection system and the spectrometer have been reported [43–45] elsewhere, and thus we will give only a brief summary here.

Polarized protons with laboratory energy $E_p=647$ MeV were scattered from $^{194,196}Pt$ targets. The particles after scattering went through a QDD arrangement (a quadrupole focusing magnet followed by two 75° bend dipole magnets) before being detected at the focal plane. The detector system consisted of two multiwire drift chambers (MWDC's) [46] to obtain the particle position information followed by plastic scintillators for timing and particle identification. The MWDC's had an active area of 10×60 cm^2 and allowed for a 0.25-mm position resolution. Typical chamber operating efficiency was found to be approximately 80%. The polarization of the beam was monitored by two independent methods. In the first, a direct method [47], a beam-line polarimeter was placed ~5 m upstream of the target. The polarimeter consisted of a CH_2 target cell and four pairs of conjugate detectors to measure the left-right asymmetry in protons scattered from hydrogen. The second way of measuring beam polarization is known as the "quench-ratio" method [48]. Here the polarization of the beam is alternately suppressed at the source, and the ratio of the beam intensities of the polarized and quenched beams is used to determine the beam polarization. The average beam polarization during the experiment using these two methods was found to be 82%. The beam spin direction was reversed about every half a minute to get a uniform sampling of both polarization states. The relative beam intensity was monitored continuously by two ionization chambers located about 1 m downstream of the target inside the scattering chamber. This was then calibrated against a Faraday cup that was placed several meters downstream of the target. Typical beam intensity on the targets was about 1 nA.

The targets employed in the experiment were self-supporting foils of platinum: for ^{194}Pt, $(99.2\pm0.5)\%$, $\rho x=30.15$ mg/cm^2, and for ^{196}Pt, $(99.15\pm0.14)\%$, $\rho x=29.62$ mg/cm^2. The overall energy resolution varied between 50 and 65 keV for ^{194}Pt and between 61 and 74 keV for ^{196}Pt.

The data were acquired in steps of $\Delta\theta=2°$ from $\theta_L=3°$ to 21°. Since the angular acceptance of the HRS is about 2.5°, this ensured a good overlap of data. During off-line analysis, for each angle, the data were binned into three equal-size angle bins ($\sim0.7°$ wide). Sample spectra obtained for $^{194,196}Pt$ are shown in Figs. 1(a) and 1(b). Several well-resolved low-lying 4^{+} states can be seen in

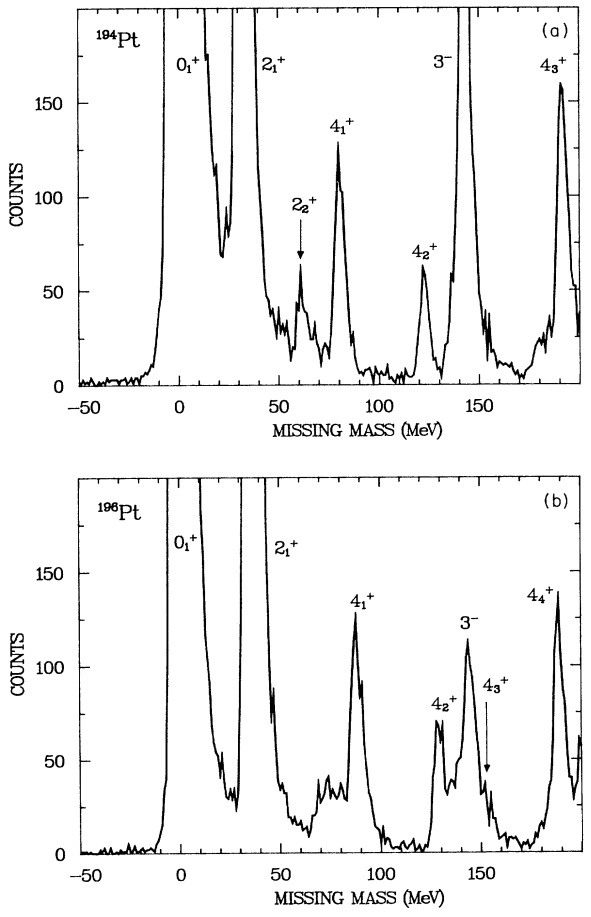

FIG. 1. (a) Spectra of protons scattered from ^{194}Pt at $\theta_L=15°$ (spin up). (b) Same as (a), but for ^{196}Pt at $\theta_L=17°$ (spin up).

both spectra. In ^{194}Pt, three 4^+ states at $E_x=0.811$, 1.229, and 1.911 MeV were observed, whereas four 4^+ states at $E_x=0.877$, 1.293, 1.537, and 1.887 MeV were excited in ^{196}Pt.

The data reduction was done using a peak-fitting program LOAF [49]. The program LOAF uses the least-squares method to fit up to ten peaks in a spectrum to any given peak shape. Any offending contaminants in the spectra were next fitted as separate peaks using another more sophisticated peak-fitting program NEWFIT [50]. The counts under these peaks were later subtracted from the states of interest. At small angles between 5° and 10°, for weak states such as the 2_2^+ and for the high-spin states which peak at larger angles, the contaminants dominated the statistics and hence some of the data at these angles were determined to be too unreliable to be of any use in the analysis. Absolute normalization of the cross-section data was obtained by taking elastic (p,p) data at several angles on a CH_2 target and normalizing these to the p-p cross sections calculated by Arndt and Roper (program SAID) [51]. The (p,p) elastic runs were repeated for several CH_2 targets and the results added to get better precision in normalization calculations. The elastic data were taken at 7° and 9° since these angles correspond to the flat regions in the elastic p-p cross section.

The plots of the angular distributions for the elastic and low-lying inelastic states are given in Figs. 2–13. The absolute cross sections are estimated to be good to ±10%. The error bars in the data represent statistical uncertainty only.

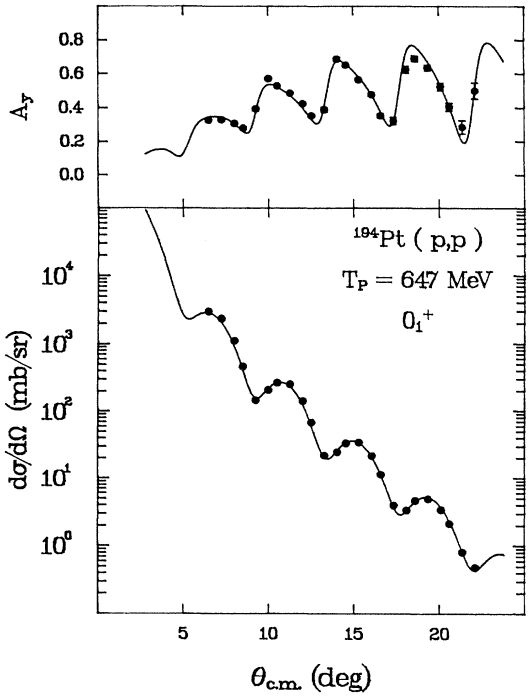

FIG. 2. Coupled-channels fits to the elastic cross-section and analyzing power data of ^{194}Pt.

III. DATA ANALYSIS

A. General

The experimental data were analyzed within the framework of the coupled-channels scheme using the program ECIS [52]. As a first step, the optical-model parameters were determined by searching on the elastic cross-section and analyzing power data with the program RELOM [53]. The optical potential was assumed to have a Woods-Saxon shape and included both real and imaginary spin-orbit terms:

$$U(r,\theta,\phi)= V(r,r_0,a)+iWf(r,r_0',a') - (V_{ls}+iW_{ls})\left[\frac{\hbar}{m_\pi c}\right]^2(\sigma\cdot l)\frac{2}{r} \times\frac{d}{dr}f(r,r_{ls},a_{ls})+V_C(r)\ , \quad (1)$$

where

$$f(r,r_x,a_x)=[1+\exp(r-R_x)/a_x]^{-1} \quad (2a)$$

and

$$R_x(\theta,\phi)=r_x A^{1/3}\left[1+\sum_\lambda \beta_\lambda Y_{\lambda 0}(\theta')\right]\ . \quad (2b)$$

The Coulomb potential $V_C(r)$ is that due to a uniformly charged sphere with a radius $R_c=1.20A^{1/3}$.

The above ten optical-model parameters were determined as follows. The elastic cross-section data were found to have extremely small statistical errors. Therefore, in the search process, these statistical uncertainties were uniformly increased by 5% to avoid having the searches dominated by the cross-section data. The optical parameters were separately searched in various combinations to obtain the lowest possible value of χ^2. Several sets of parameters giving almost equally good visual fits to the data were obtained for both ^{194,196}Pt. These are given in Table I along with the χ^2 value for

TABLE I. Optical-model parameters for ^{194,196}Pt. Units are given in fm for lengths and MeV for potentials.

A	Set	V	r_0	a	W	r_0'	a'	V_{ls}	W_{ls}	r_{ls}	a_{ls}	χ^2/N
194	I	−0.102	1.769	0.008	−58.553	1.084	0.621	−1.143	−0.366	1.079	0.834	6.6
	II	14.51	1.094	0.344	−46.661	1.117	0.601	−1.109	−0.046	1.098	0.817	3.6
	III	3.778	1.155	0.002	−54.619	1.093	0.617	−1.038	−0.172	1.105	0.807	5.4
196	I	1.748	1.139	0.003	−51.979	1.100	0.603	−1.002	−0.256	1.099	0.804	6.3
	II	6.865	1.134	0.253	−47.160	1.106	0.616	−0.843	−0.190	1.132	0.778	4.3

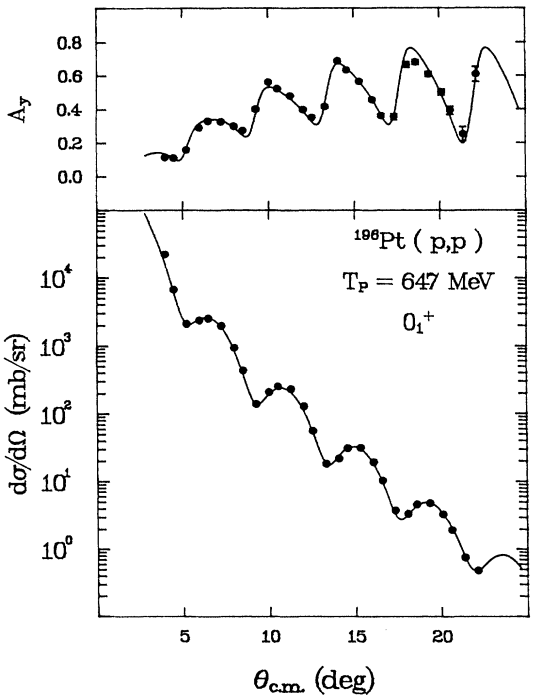

FIG. 3. Same as Fig. 2, but for ^{196}Pt.

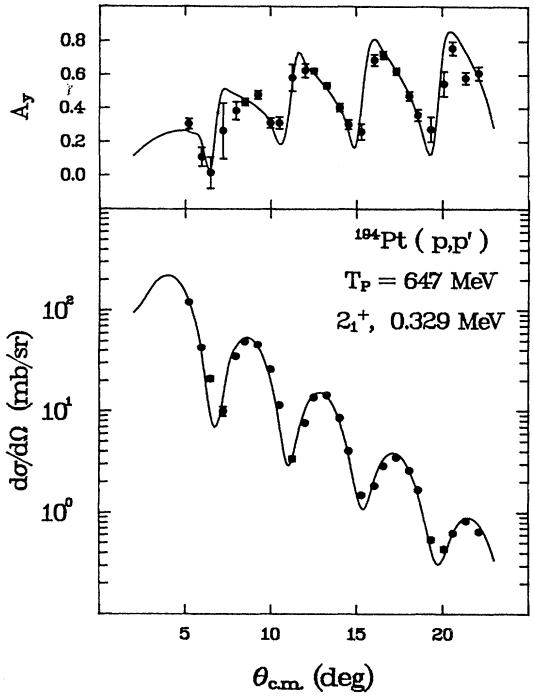

FIG. 4. Coupled-channels ($0_1^+/2_1^+$) fits to the cross-section and analyzing power data for the 2_1^+ (0.329-MeV) state of ^{194}Pt.

each set. In the subsequent analysis, the optical parameter set corresponding to the lowest χ^2/N value (set II for both isotopes) was used. Quite good fits to the elastic σ and A_y data were obtained with these parameters as shown in Figs. 2 and 3.

With the above optical-model parameters, the coupled-channels calculations were performed next. Throughout these calculations, except otherwise noted, first-order dU/dr form factors were used for the inelastic transitions.

B. Ground-state band

The ground-state band was analyzed as follows. As a first step, the deformation parameters for the 2_1^+ state were determined. Using the program ECIS, the σ and A_y

TABLE II. $E2$ matrix elements used in the coupled-channels analysis. Units are e fm^2.

		2_1	2_2	4_1	4_2	4_3	4_4
^{194}Pt	0_1	135.6[a]	−10.1[a]				
	2_1	−79[b]	145.5[b]	186.4[c]	−6.6[c]		
	2_2		76.1[c]	0[c]	−171.6[c]		
	4_1			−88.5[c]	0[c]		
	4_2				23.2[c]		
	4_3					44.8[c]	
^{196}Pt	0_1	131.2[a]	10.5[c]				
	2_1	−69.3[b]	139.8[c]	199.6[c]	−16.7[c]		
	2_2		36.0[c]	−10.2[c]	−148.7[c]	−17.7[c]	6.5[c]
	4_1			−73.7[c]	−134.8[c]	7.2[c]	−10.9[c]
	4_2				8.0[c]	129.8[c]	4.7[c]
	4_3					21.5[c]	58.7[c]
	4_4						−195.0[c]

[a]This experiment.
[b]Coulomb excitation, Refs. [4–6].
[c]IBM calculation.

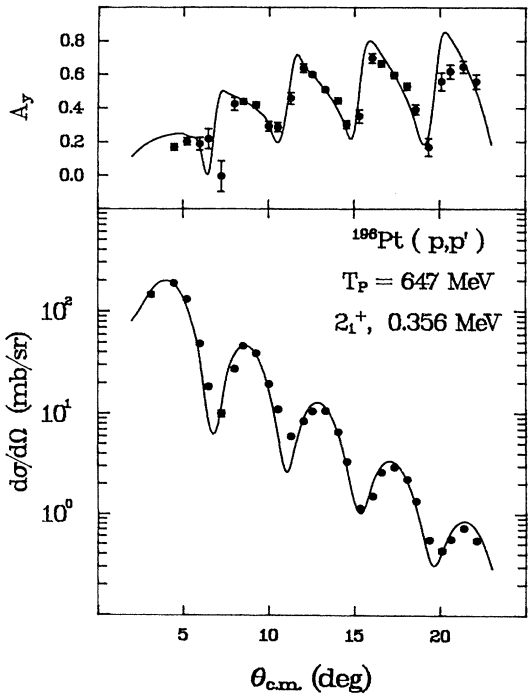

FIG. 5. Same as Fig. 4, but for the 2_1^+ (0.356-MeV) state of ^{196}Pt.

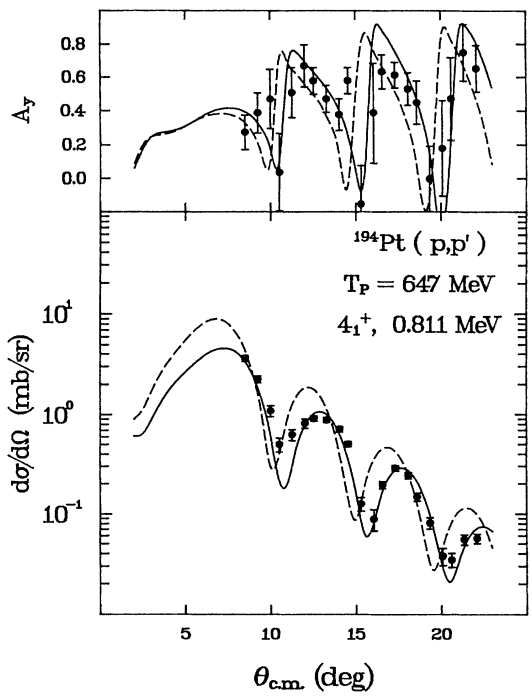

FIG. 6. Coupled-channels ($0_1^+/2_1^+/4_1^+$) fits to the cross-section and analyzing power data for the 4_1^+ (0.811-MeV) state of ^{194}Pt. For comparison are shown calculations performed with only the first-order form factor (dashed curve) and with both the first- and second-order form factors (solid curve), as described in the text.

data for the 2_1^+ state were searched in a $0_1^+/2_1^+$ coupling to obtain the β_2's. Since we have used the same geometry for the real and imaginary spin-orbit potentials, the deformations corresponding to these potentials were assumed to be the same. Quite good fits to both σ and A_y data were obtained, as shown in Figs. 4 and 5. The $E2$ matrix elements used in the analysis are shown in Table II. These have been taken either from past measurements, where available, or have been obtained from an IBM calculation. The β_2 deformation parameters obtained for the 2_1^+ state are given in Table III. Since at 647 MeV the imaginary central potential is by far the biggest part of the optical potential, it is not surprising that the imaginary central β's are the best determined in our searches for all transitions in both nuclei. For this reason, we have used this deformation parameter in the evaluation of the matrix elements to be discussed later.

With these deformations and a $0_1^+/2_1^+/4_1^+$ coupling, a search was next performed on the deformation parameters, β_4's for the 4_1^+ state. Not including the 6^+ coupling in the calculations had no significant effect on the search results. The deformation parameters obtained in an earlier ^{194}Pt study [26] were used as the initial guess in the analysis. It was found that although good fits could be obtained for the 2_1^+ state in the first-order model, the same was not the case for the 4_1^+ state. The simple first-order $\beta_2 R\,(dU/dr)$ form gave a poor fit to the 4_1^+ data, as shown in Fig. 6. However, when a second-order term

TABLE III. Deformation parameters β_λ for ^{194,196}Pt.

A	J^π	Real central	Imaginary central	Real spin-orbit	Imaginary spin-orbit
194	2_1^+	−0.206(16)	−0.161(2)	−0.168(12)	−0.168(12)
	4_1^+	−0.062(5)	−0.044(2)	−0.044(11)	−0.044(11)
	4_2^+	−0.004(5)	−0.030(1)	−0.025(4)	−0.025(4)
	4_3^+	−0.028(17)	−0.064(2)	−0.063(11)	−0.063(11)
196	2_1^+	−0.138(30)	−0.157(2)	−0.147(12)	−0.147(12)
	4_1^+	−0.040(10)	−0.041(1)	−0.035(3)	−0.035(3)
	4_2^+	−0.043(12)	−0.036(2)	−0.054(9)	−0.054(9)
	4_3^+	−0.033(7)	−0.015(1)	−0.012(5)	−0.012(5)
	4_4^+	0.006(10)	−0.046(1)	−0.047(5)	−0.047(5)

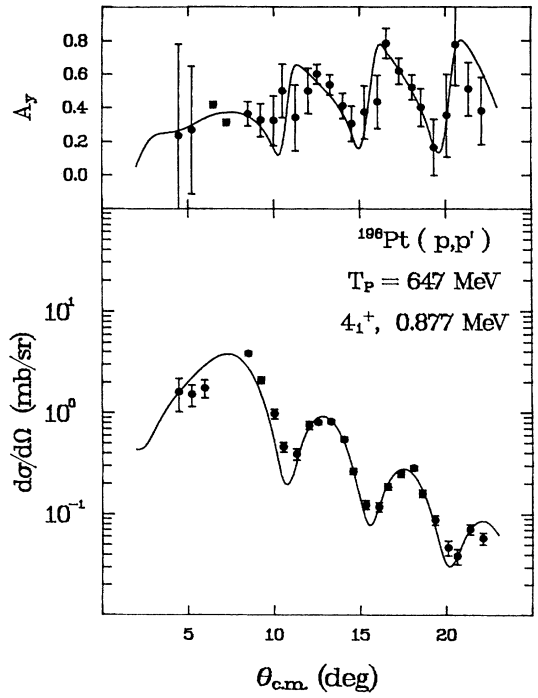

FIG. 7. Same as Fig. 6, but for the 4_1^+ (0.877-MeV) state of ^{196}Pt. Calculations shown included both first- and second-order form factors.

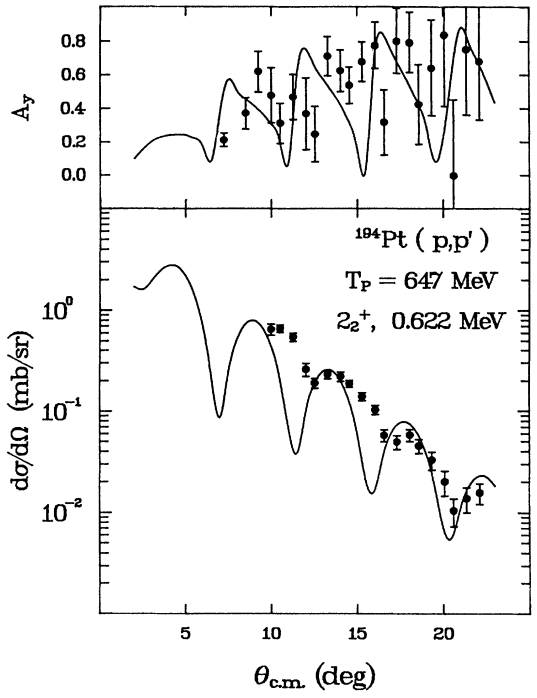

FIG. 8. Same as Fig. 4, but for the 2_2^+ (0.622-MeV) state of ^{194}Pt. The results of searching on $M^2_{0_1 2_2}$ with 2_2^+ cross-section data in a $0_1^+/2_1^+/2_2^+/4_2^+$ coupling are shown.

proportional to $\beta_2^2 R^2(d^2V/dr^2)$ was included in order to simulate the rotational model form factor, we were able to improve the fits in both phase and magnitude (see Figs. 6 and 7). This is not surprising since the 4_1^+ state belonging to the ground-state rotational band has evidently strong rotational characteristics. Except for this case, the rest of the coupled-channels analysis was done with the first-order form factor. The β_4 deformation parameters obtained in the analysis are given in Table III. As previously noted, of all four deformation parameters, the imaginary central deformation is found to have the smallest uncertainty.

C. Quasigamma band

The 2_2^+ state in both ^{194,196}Pt is quite weak. For ^{196}Pt we were unable to obtain any useful information for this state in the present experiment. In fact, for ^{196}Pt, in the IBM-1 (sd) model, the $0_1^+ \rightarrow 2_2^+$ matrix element, $M^2_{0_1 2_2}$ is predicted to be zero. In contrast, the next member of the quasigamma band, the 4_2^+ state, is quite strongly excited in both nuclei. The deformation parameters for this state were determined as follows.

In the first approximation, a search for β_4's was performed on the 4_2^+ data using a $0_1^+/2_1^+/4_2^+$ coupling. The deformations obtained for the 4_1^+ state were used as the starting guess for the 4_2^+ state. Since the interband matrix element $M^2_{2_1 4_2}$ is expected to be very small, this was

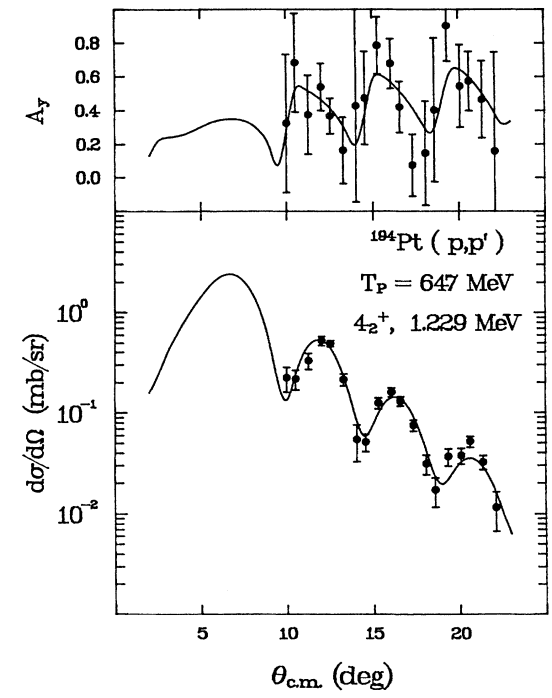

FIG. 9. Coupled-channels ($0_1^+/2_1^+/2_2^+/4_2^+$) fits to the cross-section and analyzing power data for the 4_2^+ (1.229-MeV) state of ^{194}Pt.

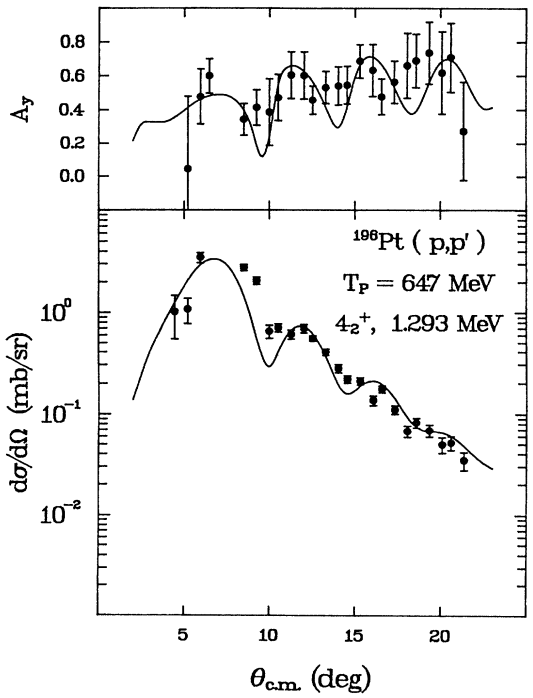

FIG. 10. Same as Fig. 9, but for the 4_2^+ (1.293-MeV) state of ^{196}Pt.

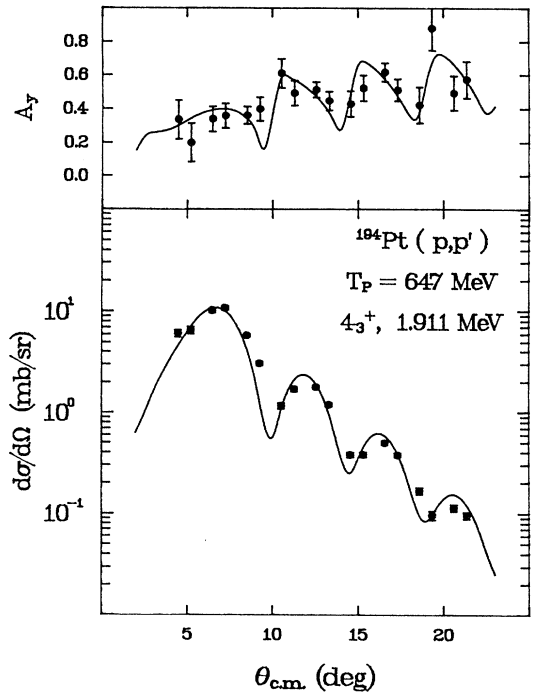

FIG. 11. Coupled-channels ($0_1^+/2_1^+/4_3^+$) fits to the cross-section and analyzing power data for the 4_3^+ (1.911-MeV) state of ^{194}Pt.

set equal to zero in the calculations. These resulting β_4's were fine tuned in a revised search using a $0_1^+/2_1^+/2_2^+/4_2^+$ coupling. The matrix element $M^2_{0_1 2_2}$ obtained in an earlier ^{194}Pt study [26] was used in the search. The $M^2_{2_2 4_2}$ value was taken from an IBM-1 calculation with a g boson. The new deformation parameters, listed in Table III, differed slightly from the ones obtained before in the $0_1^+/2_1^+/4_2^+$ search.

For ^{194}Pt the data for the 2_2^+ state were next used to search on the $M^2_{0_1 2_2}$ matrix element. The calculation was performed in a $0_1^+/2_1^+/2_2^+/4_2^+$ coupling. The value of $M^2_{0_1 2_2} = -9.8(4)\ e\,\mathrm{fm}^2$ obtained in an earlier 135-MeV $(\vec{p},p')$ experiment [26] was used as the starting guess. Since Ref. [26] is the only known determination of this matrix element's sign, both choices for the sign were investigated in the calculations. The analysis favors a negative sign for this matrix element. The result is

$$M^2_{0_1 2_2} = -10.1(4)\ e\,\mathrm{fm}^2 ,$$

in quite good agreement, in both sign and magnitude, with the value obtained in Ref. [26].

The σ and A_y fits for the 2_2^+ state are shown in Fig. 8 and for the 4_2^+ state in Figs. 9 and 10.

D. Higher 4^+ states

In contrast with the predictions of the IBM, the higher 4^+ states in the platinum isotopes are quite strongly ex-

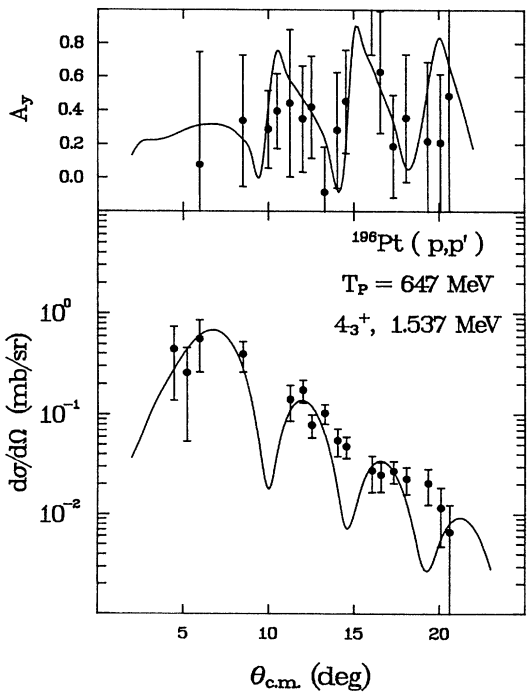

FIG. 12. Same as Fig. 11, but for the 4_3^+ (1.537-MeV) state of ^{196}Pt.

cited. We now turn to the analysis of the 4_3^+ (1.911-MeV) state in ^{194}Pt and the 4_3^+ (1.537-MeV) and 4_4^+ (1.887-MeV) states in ^{196}Pt. The 4^+ state at 1.537 MeV in ^{196}Pt has escaped observation in a number of experiments. However, it was measured by Schüler *et al.* [37] in a $(d,pn\gamma)$ study, and they interpreted it as the 4_3^+ ($\sigma=6$, $\tau=4$) state of IBM-1. We have analyzed these 4^+ states in the same spirit as the first 4^+ state. The searches on the deformation parameters for the 4^+ states were performed using a $0_1^+/2_1^+/4_i^+$ ($i=3,4$) coupling. The deformation parameters set obtained for the 4_1^+ state was used as the starting step in these searches. The real and imaginary spin-orbit deformations were considered to be equal for the reason given before. The matrix elements $M^2_{2_1 4_i}$ and $M^2_{4_i 4_i}$ given in Table II were used in the analysis. The results of these searches for β_4's are given in Table III. Quite good fits to both σ and A_y data for the 4^+ states were found as shown in Figs. 11–13.

Having determined the deformations for the states of interest, it is now straightforward to obtain the multipole matrix elements to these states. The $E\lambda$ matrix element can be written as

$$M(E\lambda)=\int_0^\infty \rho_\lambda(r) r^{\lambda+2} dr \ . \tag{3}$$

If the transition density is proportional to the derivative of the ground-state density,

$$\rho_\lambda(r)=-\beta_\lambda R_0 \frac{\partial \rho_0}{\partial r} \ , \tag{4}$$

and the deformations of the potential and the charge density are considered to be equal, then it is easy to show

$$M(E\lambda)=\frac{\lambda+2}{4\pi} ZeR_0\beta_\lambda \langle r^{\lambda-1}\rangle \ , \tag{5}$$

which, for the Woods-Saxon distribution, reduces to a simple expression [54]

$$M(E\lambda)\simeq \frac{3}{4\pi} ZeR_0^\lambda \beta_\lambda \left[1+\frac{(\lambda-1)(\lambda+4}{6}\left[\frac{\pi a}{R_0}\right]^2\right] , \tag{6}$$

where terms of higher order in (a/R_0) are ignored. This approximation should not have a significant effect in the calculations because only transitions involving relatively small values of λ are being considered.

The matrix elements obtained with Eq. (6) are generally in good agreement with those from the past measurements. In Tables IV and V, the $B(E2)$ values from different experiments are given. The agreement between present and previous measurements of the $B(E2)$'s for the 2_1^+ and 2_2^+ states is quite good.

The primary motivation of this study was to obtain the $E4$ matrix elements to the low-lying 4^+ states. These are calculated with Eq. (6) and are listed in Table VI along with other available measurements of these matrix elements. Because of significant amount of competing $E2$ transitions in the ground-state band, the sign of the $E4$

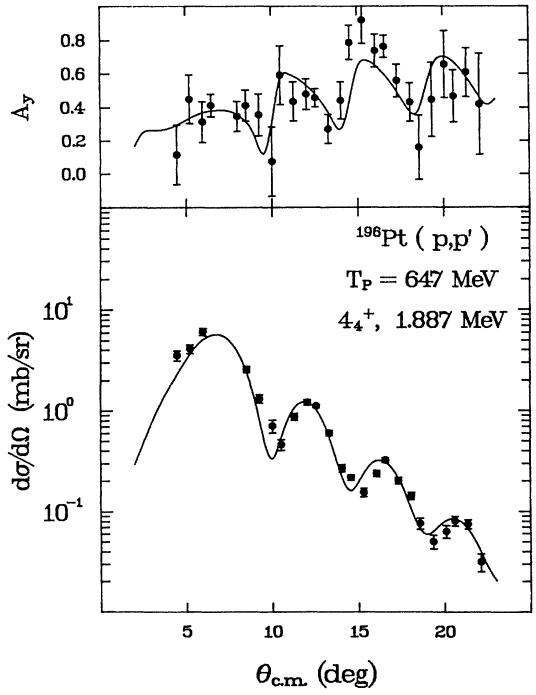

FIG. 13. Coupled-channels ($0_1^+/2_1^+/4_4^+$) fits to the cross-section and analyzing power data for the 4_4^+ (1.887-MeV) state of ^{196}Pt.

TABLE IV. Comparison of experimental $B(E2)$'s with the IBM predictions for ^{194}Pt. Units are e^2b^2.

$J_i \to J_f$	Experiment	IBM-1 (*sd*)	IBM-1 (*sdg*)
$2_1 \to 0_1$	0.368(9)[a]	0.345	0.403
	0.345(27)[b]		
	0.332(2)[c]		
	0.374(16)[d]		
	0.324(3)[e]		
$2_2 \to 0_1$	0.0020(4)[a]	0.0014	0.009
	0.0019(2)[b]		
	0.0014(2)[d]		
	0.0016(2)[e]		
$2_2 \to 2_1$	0.58(7)[d]	0.442	0.430
	0.423(15)[e]		
$4_1 \to 2_1$	0.47(3)[d]	0.462	0.572
	0.449(22)[e]		
$4_2 \to 2_1$	0.010(5)[e]	6.7×10^{-6}	5.0×10^{-4}
$4_2 \to 2_2$	0.28(12)[d]	0.255	0.327
	0.69(39)[e]		
$4_2 \to 4_1$	0.87(43)[e]	0.225	0.238
$6_1 \to 4_1$	0.32(8)[d]	0.487	0.647
$6_2 \to 4_2$	0.28(6)[d]	0.313	0.44

[a]This experiment.
[b](p,p'), Ref. [26].
[c]Coulomb excitation, Ref. [8].
[d]Coulomb excitation, Ref. [30].
[e]Coulomb excitation, Ref. [6].

TABLE V. Comparison of experimental $B(E2)$'s with the IBM predictions for ^{196}Pt. Units are e^2b^2.

$J_i \rightarrow J_f$	Experiment	IBM-1 (sd)	IBM-1 (sdg)
$2_1 \rightarrow 0_1$	0.344(9)[a]	0.270	0.315
	0.276(1)[b]		
	0.288(14)[c]		
	0.30[d]		
$2_2 \rightarrow 0_1$	3.0×10^{-6}[e]	0	2.2×10^{-3}
$2_2 \rightarrow 2_1$	0.350(31)[c]	0.354	0.391
	0.262(55)[d]		
$4_1 \rightarrow 2_1$	0.403(32)[c]	0.354	0.443
	0.443(26)[d]		
	0.38(3)[e]		
$0_2 \rightarrow 2_1$	0.033(7)[d]	0	0.006
	0.021(10)[e]		
$0_2 \rightarrow 2_2$	0.142(77)[c]	0.36	0.448
$4_2 \rightarrow 2_1$	0.003(1)[c]	0	0.003
	0.0023(8)[d]		
$4_2 \rightarrow 2_2$	0.177(35)[c]	0.189	0.246
	0.218(43)[d]		
$4_2 \rightarrow 3_1$	<0.06[e]	0	0.026
$4_2 \rightarrow 4_1$	0.193(97)[c]	0.17	0.20
	0.218(54)[d]		
	0.18(9)[e]		
$6_1 \rightarrow 4_1$	0.421(116)[c]	0.36	0.50
	0.494(37)[d]		
	0.40(11)[e]		
$6_2 \rightarrow 4_1$	0.0037(16)[d]	0	0.0022
$6_2 \rightarrow 4_2$	0.350(102)[d]	0.218	0.327

[a]This experiment.
[b]Coulomb excitation, Ref. [8].
[c]Coulomb excitation, Ref. [31].
[d]Coulomb excitation, Ref. [32].
[e](n,γ), Ref. [22].

matrix element $M^4_{0_1 4_1}$ is unambiguously determined in the coupled-channels analysis described above. However, the same is not true for the higher 4^+ states, and therefore the signs of the corresponding $E4$ matrix elements could not be deduced. For ^{194}Pt the calculated $E4$ matrix elements are in quite good agreement with the previously reported values. The $M^4_{0_1 4_1}$ and $M^4_{0_1 4_2}$ are in excellent agreement with those obtained earlier in a 135-MeV $(\vec{p},p')$ experiment (Ref. [26]). However, the present value of 2799 e fm^4 for $M^4_{0_1 4_3}$ is about 25% bigger than the value obtained in Ref. [26]. Based on the superior fit to the 4^+_3 data, we believe the present result is more reliable. No other measurement of this matrix element is available to our knowledge. The $E4$ matrix elements given in Ref. [26] differ somewhat from the values quoted in Table VI because the latter have been recalculated using Eq. (6). Three of the four 4^+ states in ^{196}Pt measured in this experiment have also been observed in an (e,e') experiment [39]. As shown in Table VI, there is quite good agreement between the (e,e') and (p,p') results for the $E4$ matrix elements. We next analyze these results in the context of the interacting boson model.

IV. IBM ANALYSIS

A. IBM-1 (sd)

A simple IBM-1 Hamiltonian suitable for the Pt-Os region and consisting of s and d bosons only can be written as [55]

$$H = a_1 \hat{\mathbf{L}}\cdot\hat{\mathbf{L}} + a_2 \hat{\mathbf{Q}}\cdot\hat{\mathbf{Q}} , \tag{7}$$

where the multipole representation [56] of H has been used. If we constrain H to include a maximum of two-

TABLE VI. Comparison of experimental $E4$ matrix with the IBM predictions. Units are e fm^4.

	^{194}Pt		^{196}Pt	
$M^4_{0_1 4_i}$	Experiment	IBM-1 (sd)	Experiment	IBM-1 (sd)
$M^4_{0_1 4_1}$	$-1914(92)$[a]	-1914[b]	$-1754(65)$[a]	-1754[b]
	$-1953(67)$[c]		$\pm1549(161)$[d]	
	$\pm2300(800)$[e]		$\pm1800(700)$[e]	
$M^4_{0_1 4_2}$	$\pm1307(55)$[a]	-85	$\pm1572(86)$[a]	0
	$\pm1145(67)$[c]		$\pm1414(142)$[d]	
	$\pm1300(300)$[e]		<1400[e]	
$M^4_{0_1 4_3}$	$\pm2799(100)$[a]	-0.8	$\pm670(56)$[a]	0
	$\pm2290(67)$[c]			
$M^4_{0_1 4_4}$			$\pm1996(48)$[a]	247
			$\pm2098(313)$[d]	

[a]This experiment.
[b]$E4$ effective charges adjusted to fit this matrix element.
[c](p,p'), Ref. [26].
[d](e,e'), Ref. [39].
[e]Coulomb excitation, Refs. [6,8].

body interactions, then the angular momentum operator $\hat{\mathbf{L}}$ and the quadrupole moment operator $\hat{\mathbf{Q}}$ take the following form:

$$\hat{\mathbf{L}}=(d^{\dagger}\tilde{d})^{(1)}\ ,$$
$$\hat{\mathbf{Q}}=(d^{\dagger}s+s^{\dagger}\tilde{d})^{(2)}+\chi_{dd}(d^{\dagger}\tilde{d})^{(2)}\ , \tag{8}$$

where $d^{\dagger}$ and $\tilde{d}$ are the d-boson creation and annihilation operators, respectively, and the superscripts on the operators denote their tensor rank. The above Hamiltonian was diagonalized in the sd-boson basis space to obtain the corresponding eigenfunctions using the computer program PHINT [57]. These eigenfunctions were next used to calculate the transition rates with the following electric operators:

$$T(E2)=q[(d^{\dagger}s+s^{\dagger}\tilde{d})^{(2)}+\chi_{dd}(d^{\dagger}\tilde{d})^{(2)}]\ ,$$
$$T(E4)=h(d^{\dagger}\tilde{d})^{(4)}\ . \tag{9}$$

Since the same quadrupole operator is used in both the H and $T(E2)$, the above parametrization is called the "consistent Q formalism" (CQF) [55]. The CQF leads to considerable simplicity in describing the transition region as the number of parameters involved is greatly reduced. The $\hat{\mathbf{L}}\cdot\hat{\mathbf{L}}$ term is diagonal in the basis space and does not affect the wave functions and transition rates. The parameters a_2 and q simply scale the eigenvalues and $B(E2)$ values. So the Pt-Os transition region can be described essentially by varying a single parameter χ_{dd}. Corresponding to the two limits O(6) and SU(3), χ_{dd} takes on the values 0 and $-\frac{1}{2}\sqrt{7}$, respectively. The values of χ_{dd} between these two limits describe the entire transition region O(6)$\rightarrow$SU(3). For a given nucleus, the parameter χ_{dd} is obtained by fitting the experimental branching ratio

$$R=\frac{B(E2,2_2^+\rightarrow 0_1^+)}{B(E2,2_2^+\rightarrow 2_1^+)}\ . \tag{10}$$

$\chi_{dd}=0.4$ and 0.0 were found to best describe ^{194}Pt and ^{196}Pt, respectively. The predictions of this model are compared with the experimental matrix elements from different sources in Tables IV–VI. The agreement between experiment and IBM-1 for the $E2$ matrix elements is quite good in general and this represents but a sample of the trend found across the Pt-Os region [24]. Specifically, for ^{194}Pt the agreement is excellent for the low-lying states, but deteriorates somewhat as one moves up in the excitation energy and toward high-spin states. For ^{196}Pt, again, there is overall good agreement with the experiment. However, there are a few exceptions that are worth mentioning. Let us look at some special cases in ^{196}Pt. The matrix element $M^2_{0_1 2_2}$ is predicted to be zero in the IBM-1, whereas experimentally it has a nonvanishing, albeit small, value. Similarly, the quadrupole moment of the 2_1^+ state (not shown) is zero in the IBM-1 limit, but it has been found to have a large nonzero value in several experiments [4,5,8]. It is also interesting to compare the properties of the excited 0^+ state for ^{196}Pt. These states are known to display quite contrasting behavior in the Pt-Os region and thus provide interesting tests of a model candidate. In the Pt isotopes, the excited 0^+ states decay both to the 2_1^+ and 2_2^+ states, whereas in the Os isotopes they predominantly populate the 2_2^+ state. The disagreement between the experiment and IBM-1 with respect to the excited 0^+ state is noticeable.

We next consider the excitation of the $E4$ states. In the IBM-1 (sd), there is only one way to excite a 4^+ state, i.e., through the operator $h(d^{\dagger}\tilde{d})^{(4)}$. In the calculations the effective charge h was varied until $M^4_{0_1 4_1}$ was reproduced. The required values of h were found to be -574 and -596 e fm^4 for ^{194}Pt and ^{196}Pt, respectively. The $E4$ matrix elements predictions for the higher 4^+ states in this scheme are given in Table VI. It is clear that the IBM-1 with sd bosons is unable to give large strengths found experimentally for these states, and thus one must look for improvements in the model.

There are two chief criticisms of the IBM-1: first, that the restriction limiting the model to include only s and d bosons is too severe, and second, treating the proton and neutron bosons as identical is too naive and unphysical. The former is overcome by including additional degrees of freedom (such as a g boson) [25,26] in the model, while a more sophisticated approach (IBM-2) [58,59], in which proton and neutron bosons are treated separately, is used to remove the latter shortcoming. Here we study the first of these two refinements, namely, the inclusion of g bosons in the IBM-1. Some examples of an IBM-2 approach to study these nuclei can be found elsewhere [26,60–62].

B. IBM-1 (sdg)

The inability of the IBM-1 (sd) model to predict the observed large $E4$ strengths in ^{194,196}Pt makes the g boson a logical choice for the extra degree of freedom which must be introduced in the model. The motivation for such a modification does not come from Pt isotopes alone. There is additional experimental evidence in the form of low-lying $K=4$ bands in the Os isotopes which makes a strong case for the need for the g bosons [25].

The effects of including the g bosons were first worked out in a perturbational approach by Sage and Barrett [63]. Several studies [64–77] have since been done to investigate the importance of the g bosons. Although there has been some indication [76] that Pauli corrections to the $E4$ operator may be at least as important, there seems to be overwhelming justification for including the g bosons in the IBM. Recently, Boeglin *et al.* [77] measured transition charge densities using electron scattering for the low-lying levels in several Os-Pt isotopes and compared their results with the IBM predictions. They show that even when IBM-2 is invoked it is necessary to include a g boson to successfully explain the measured transition densities for the 4^+ states.

To study the importance of the g bosons, the basis space was expanded to sdg bosons and the Hamiltonian was diagonalized in this basis [67,68]. The Hamiltonian allowing for at most one g bosons can be written as

$$H=a_1\hat{\mathbf{L}}\cdot\hat{\mathbf{L}}+a_2\hat{\mathbf{Q}}\cdot\hat{\mathbf{Q}}+\epsilon_g\hat{\mathbf{n}}_g \tag{11}$$

where

TABLE VII. $E2$ parameters used in the IBM-1 (sdg) model.

A	q (e fm^2)	ϵ_g (MeV)	χ_{dd}	χ_{gd}	χ_{gg}
194	15.0	1.5	0.04	1.7	1.5
196	15.0	1.5	0.0	1.5	2.6

$$\hat{\mathbf{n}}_g=(g^\dagger\tilde{g})^{(0)}\ ,$$
$$\hat{\mathbf{L}}=(d^\dagger\tilde{d})^{(1)}\ , \tag{12}$$
$$\hat{\mathbf{Q}}=(d^\dagger s+s^\dagger\tilde{d})^{(2)}+\chi_{dd}(d^\dagger\tilde{d})^{(2)}+\chi_{gd}(g^\dagger\tilde{d}+d^\dagger\tilde{g})^{(2)}+\chi_{gg}(g^\dagger\tilde{g})^{(2)}\ .$$

The $E2$ transition operator using the CQF can be parametrized as before:

$$T(E2)=q\hat{\mathbf{Q}}\ . \tag{13}$$

With the inclusion of a g boson, some of the simplicity of the IBM-1 (sd) model is lost, and there are additional g-boson-related parameters to deal with. However, some simplifications emerge and are easy to see. The $E2$ properties were found to be insensitive to the g-boson terms. So all the sd boson $E2$ parameters were left at their original values. In subsequent calculations, therefore, the g-boson terms were exclusively used to reproduce the $E4$ data. The g-boson parameters were determined as follows.

Since in the IBM-1 (sd) scheme the higher 4^+ states are poorly described, for the present calculations, the 4^+ state around 1.9 MeV in both isotopes was treated as consisting of mostly g-boson configurations. It was found during our analysis that the parameter χ_{gg} only changed the energy of the g-boson levels, whereas χ_{gd} was responsible for the g-boson admixtures in the sd-boson states. Therefore, with $\chi_{gd}=0$, we adjusted χ_{gg} to obtain a pure g-boson state at approximately 1.9 MeV excitation energy. The mixing parameter χ_{gd} was set at 1.5, a value necessary to obtain about 10–20% g-boson configurations in the pure sd-boson lower 4^+ states in both nuclei. Finally, ϵ_g was taken to be 1.5 MeV, a value appropriate for the pairing gap in the region.

With these parameters the modified IBM-1 calculations were performed. The results for the $E2$ matrix elements are given in Tables IV and V. The new $E2$ predictions are still in good agreement with the data, and in some cases, for example, the high-spin states in ^{196}Pt, the agreement is even improved compared to the pure sd scheme. This is not surprising, for the effects of a g-boson should be most evident in high-spin states. The $E2$ parameters used are given in Table VII.

We next turn to the $E4$ properties. The sdg-boson $E4$ transition operator can be written as

$$T(E4)=h[(g^\dagger s+s^\dagger\tilde{g})^{(4)}+\eta_{dd}(d^\dagger\tilde{d})^{(4)}+\eta_{gd}(g^\dagger\tilde{d}+d^\dagger\tilde{g})^{(4)}+\eta_{gg}(g^\dagger\tilde{g})^{(4)}]\ . \tag{14}$$

The $E4$ transition operator now has four terms instead of just one in the sd scheme. One therefore has the freedom in the sdg scheme of varying the parameters h, η_{dd}, η_{gd}, and η_{gg} to fit the measured $B(E4)$'s. Since there are very few g-boson configurations in the ground state, the η_{gg} term is expected to be ineffective in causing $0_1^+\rightarrow 4_i^+$ excitations and, hence, was dropped in the analysis. The remaining three parameters h, η_{dd}, and η_{gd} were then adjusted to obtain a good fit to the $E4$ matrix elements. For ^{194}Pt there are three measured matrix elements $M^4_{0_1 4_i}$ ($i=1,2,3$). Of these, the sign of only $M^4_{0_1 4_1}$ is known. Therefore, we considered all four sign combinations for the matrix elements. The results of the parameter search are shown in Table VIII. For ^{196}Pt a similar analysis was performed to find the $E4$ effective charges. As expected, the effective charge parameters for the two neighboring isotopes ^{194,196}Pt are very similar. Since we were able to measure four 4^+ states in ^{196}Pt, the additional 4^+ state could be used for a consistency check of the method described above. The 4_4^+ state at 1.887 MeV was considered as the dominant g-boson state. Using the three most strongly excited 4^+ states (4_1^+, 4_2^+, and 4_4^+), the $E4$ effective charges were determined, and these were used to predict the $E4$ matrix elements for the 4_3^+ state. The present experimental value for $M^4_{0_1 4_3}$ from this experiment is $\pm 670\pm 56$ e fm^4. Using the $E4$ effective charge solutions corresponding to the $(-/-/-)$ sign combination for the 4_1^+, 4_2^+, and 4_4^+ states (see Table VIII), we obtain $M^4_{0_1 4_3}=-580$ e fm^4, in reasonable agreement with the experimental value. Borghols *et al.* [39] have measured the transition densities for the 4_1^+, 4_2^+, and 4_4^+ states of ^{196}Pt in an (e,e') experiment and then used the results in an IBM-2 framework to predict the $E4$ moment for the third 4^+ state. They find $M^4_{0_1 4_3}=\pm 778\pm 88$ e fm^4,

TABLE VIII. $E4$ effective charge parameters for ^{194,196}Pt. Units are in e fm^4.

	^{194}Pt			^{196}Pt		
$s_1/s_2/s_k$[a]	h	η_{dd}	η_{gd}	h	η_{dd}	η_{gd}
$-/-/-$	−349.3	0.44	4.22	−239.1	0.79	6.70
$-/-/+$	1197.0	−0.89	−1.84	1284.0	−0.91	−2.21
$-/+/-$	−1163.0	−0.02	−1.14	−1291.6	−0.09	−1.64
$-/+/+$	383.0	−2.30	2.23	232.3	−3.71	3.81

[a] s_i denotes the sign of $M^4_{0_1 4_i}$. $k=3$ for ^{194}Pt and $k=4$ for ^{196}Pt.

which is in fairly good agreement with our results.

Finally, it is interesting to note that only one set of $E4$ effective charges corresponding to $(-/-/-)$ sign combination for the matrix elements of 4_1^+, 4_2^+, and 4_4^+ states was able to give good agreement with the measured $E4$ matrix elements for the 4_3^+ state—an indication that only one set of sign combinations is physically meaningful.

V. CONCLUSIONS

We have investigated the two platinum isotopes ^{194,196}Pt using inelastic proton scattering at 647 MeV. The main focus of this investigation has been the excitation of the low-lying 4^+ states in these nuclei. A total of seven 4^+ states have been found below 2 MeV in ^{194}Pt and ^{196}Pt. Large $E4$ moments to these states were obtained from the coupled-channels analysis of the data. The results are in quite good agreement with earlier $(p,p')$and (e,e') studies.

These results were next compared with the predictions of the IBM-1 using a Hamiltonian appropriate for the Pt-Os transition region. The CQF was used throughout the calculations. The IBM-1 (sd) results, although in quite good accord with the $E2$ systematics found in these nuclei, were in sharp disagreement with the large $E4$ strengths observed. When a g boson was included in the model, it was possible to give a reasonable description of the $E4$ matrix elements. In addition, the good agreement for the $E2$ matrix elements found in the sd scheme was retained, and in some cases this agreement was even improved, e.g., the high-spin states in ^{196}Pt. We have therefore shown that any successful attempts at describing the $E4$ matrix elements, within an IBM framework, must include higher degree of freedom, e.g., g bosons.

ACKNOWLEDGMENTS

We would like to thank D. Ciskowski for help during data taking. We also greatly appreciate many helpful discussions with Prof. F. Todd Baker, Prof. O. Scholten, and Prof. P. Van Isacker. This work was supported by the Department of Energy under Grant No. DE-FG02-88ER40405 A002 and the Minnesota Supercomputer Institute.

[1] R. J. Pryor and J. X. Saladin, Phys. Rev. C **1**, 1573 (1970).
[2] S. A. Lane and J. X. Saladin, Phys. Rev. C **6**, 613 (1972).
[3] C. Baktash, J. X. Saladin, J. J. O'Brien, and J. G. Alessi, Phys. Rev. C **22**, 2383 (1980).
[4] J. E. Glenn and J. X. Saladin, Phys. Rev. Lett. **20**, 1298 (1968).
[5] J. E. Glenn, R. J. Pryor, and J. X. Saladin, Phys. Rev. **188**, 1905 (1969).
[6] C. Baktash, J. X. Saladin, J. J. O'Brien, and J. G. Alessi, Phys. Rev. C **18**, 131 (1978).
[7] C. Y. Chen, J. X. Saladin, and A. A. Hussein, Phys. Rev. C **28**, 1570 (1983).
[8] G. J. Gyapong, R. H. Spear, M. T. Esat, M. P. Fewell, A. M. Baxter, and S. M. Burnett, Nucl. Phys. **A458**, 165 (1986).
[9] A. S. Davydov and G. F. Filippov, Nucl. Phys. **8**, 237 (1958).
[10] R. Sahu, Phys. Rev. C **29**, 1486 (1984).
[11] A. Faessler, W. Greiner, and R. K. Sheline, Nucl. Phys. **70**, 33 (1965); see also J. M. Eisenberg and W. Greiner, *Nuclear Models* (North-Holland, Amsterdam, 1970), Vol. II, Chap. 6.
[12] A. S. Davydov and A. A. Chaban, Nucl. Phys. **20**, 499 (1960); A. S. Davydov, *ibid.* **24**, 682 (1961).
[13] L. Wilets and M. Jean, Phys. Rev. **102**, 788 (1956).
[14] H. Toki and A. Faessler, Z. Phys. A **276**, 35 (1976).
[15] F. Todd Baker, Phys. Rev. Lett. **43**, 195 (1979); Nucl. Phys. **A331**, 39 (1979).
[16] R. Sedlmayer, M. Sedlmayer, and W. Greiner, Nucl. Phys. **A232**, 465 (1974); R. Sedlmayer, M. Sedlmayer, and H. Stock, *ibid.* **A303**, 393 (1978); G. Gneuss and W. Greiner, *ibid.* **A171**, 449 (1971).
[17] K. Kumar and M. Baranger, Nucl. Phys. **A110**, 529 (1968); *ibid.* **A122**, 273 (1968); K. Kumar, Phys. Rev. C **1**, 369 (1970).
[18] U. Götz, H. C. Pauli, K. Alder, and K. Junker, Nucl. Phys. **A192**, 1 (1972).
[19] K. J. Weeks and T. Tamura, Phys. Rev. Lett. **44**, 533 (1980); Phys. Rev. C **22**, 533 (1980).
[20] A. Arima and F. Iachello, Phys. Rev. Lett. **35**, 1069 (1975); Ann. Phys. (N.Y.) **99**, 253 (1976); **111**, 201 (1978); Phys. Rev. Lett. **40**, 385 (1978); Ann. Phys. (N.Y.) **123**, 468 (1979); Annu. Rev. Nucl. Part. Sci. **31**, 75 (1981).
[21] R. F. Casten and D. D. Warner, Rev. Mod. Phys. **60**, 389 (1988).
[22] J. A. Cizewski, R. F. Casten, G. J. Smith, M. L. Stelts, W. R. Kane, H. G. Borner, and W. F. Davidson, Phys. Rev. Lett. **40**, 167 (1978).
[23] J. A. Cizewski, R. F. Casten, G. J. Smith, M. R. Macphail, M. L. Stelts, W. R. Kane, H. G. Borner, and W. F. Davidson, Nucl. Phys. **A323**, 349 (1979).
[24] R. F. Casten and J. A. Cizewski, Nucl. Phys. **A309**, 477 (1978).
[25] F. Todd Baker, A. Sethi, V. Penumetcha, G. T. Emery, W. P. Jones, and M. A. Grim, Jr., Phys. Rev. C **32**, 2212 (1985).
[26] A. Sethi, F. Todd Baker, G. T. Emery, W. P. Jones, and M. A. Grimm, Jr., Nucl. Phys. **A518**, 536 (1990).
[27] W. T. Milner, F. K. McGowan, R. L. Robinson, P. H. Stelson, and R. O. Sayer, Nucl. Phys. **A177**, 1 (1971).
[28] J. Halpern, Nucl. Data Sheets **28**, 485 (1979).
[29] I. Y. Lee, D. Cline, P. A. Butler, R. M. Diamond, J. O. Newton, R. S. Simon, and F. S. Stephens, Phys. Rev. Lett. **39**, 684 (1977).
[30] K. Stelzer, F. Rauch, Th. W. Elze, Ch. E. Gould, J. Idzko, G. E. Mitchell, H. Nottrodt, R. Zoller, H. J. Wollersheim, and H. Emling, Phys. Lett. **70B**, 297 (1977).
[31] H. H. Bolotin, A. E. Stuchbery, I. Morrison, D. L. Kennedy, C. G. Ryan, and S. H. Sie, Nucl. Phys. **A370**, 146 (1981).
[32] A. Mauthofer, K. Stelzer, J. Idzko, Th. W. Elze, H. J. Wollersheim, H. Emling, P. Fuchs, E. Grosse, and D. Schwalm, Z. Phys. A **336**, 263 (1990).
[33] J. F. W. Jansen and H. Pauw, Nucl. Phys. **A94**, 235 (1967).

[34] J. F. W. Jansen, H. Pauw, and C. J. Toeset, Nucl. Phys. **A115**, 321 (1968).
[35] I. Berkes, R. Rougny, Michele Meyer-Levy, J. Daniere, G. Lhersonneau, and A. Troncy, Phys. Rev. C **6**, 1098 (1972).
[36] H. Ton, G. H. Dulfer, J. Brasz, R. Kroondijk, and J. Blok, Nucl. Phys. **A153**, 129 (1970).
[37] P. Schüler, J. Recht, H. Wilzek, K. Hardt, C. Gunther, K. P. Blume, K. Euler, and V. Kölschbach, Z. Phys. A **317**, 313 (1984).
[38] P. T. Deason, C. H. King, T. L. Khoo, J. A. Nolen, Jr., and F. M. Bernthal, Phys. Rev. C **20**, 927 (1979).
[39] W. T. A. Borghols, N. Blasi, R. Bijker, M. N. Harakeh, C. W. De Jager, J. B. Van Der Laan, H. De Vries, and S. Y. Van Der Werf, Phys. Lett. **152B**, 330 (1985).
[40] P. T. Deason, C. H. King, R. M. Ronningen, T. L. Khoo, F. M. Bernthal, and J. A. Nolen, Jr., Phys. Rev. C **23**, 1414 (1981).
[41] F. Todd Baker, Alan Scott, T. H. Kruse, W. Hartwig, E. Ventura, and W. Savin, Nucl. Phys. **A266**, 337 (1976).
[42] F. Todd Baker, Alan Scott, T. P. Cleary, J. L. C. Ford, E. E. Gross, and D. C. Hensley, Nucl. Phys. **A321**, 222 (1979).
[43] R. Rolfe, Los Alamos National Laboratory Scientific Report No. LA-6631-T, 1976 (unpublished).
[44] G. S. Blanpied, W. R. Coker, R. P. Liljestrand, R. L. Ray, G. W. Hoffmann, D. Madland, C. L. Morris, J. C. Pratt, J. E. Spencer, H. A. Thiessen, N. M. Hintz, G. S. Kyle, M. A. Oothoudt, T. S. Bauer, J. C. Fong, G. Igo, R. J. Ridge, C. A. Whitten, Jr., T. Kozlowski, D. K. McDaniels, P. Varghese, P. M. Lang, H. Nann, K. K. Seth, and C. Glashausser, Phys. Rev. Lett. **39**, 1447 (1977).
[45] G. W. Hoffmann, L. Ray, M. Barlett, J. McGill, G. S. Adams, G. J. Igo, F. Irom, A. T. M. Wang, C. A. Whitten, Jr., R. L. Boudrie, J. F. Amann, C. Glashausser, N. M. Hintz, G. S. Kyle, and G. S. Blanpied, Phys. Rev. C **21**, 1488 (1980).
[46] L. G. Atencio, J. A. Amann, R. L. Boudrie, and C. L. Morris, Nucl. Instrum. Methods **187**, 381 (1981).
[47] M. W. McNaughton, P. R. Bevington, H. B. Willard, E. Winkelmann, E. P. Chamberlin, F. H. Cverna, N. S. P. King, and H. Wilmes, Phys. Rev. C **23**, 1128 (1981).
[48] G. G. Ohlsen, Los Alamos National Laboratory Report No. LA-4451, 1970.
[49] L. E. Smith, computer code LOAF, 1983 (unpublished).
[50] C. L. Morris, computer code NEWFIT (unpublished).
[51] R. A. Arndt and D. Roper, VPI and SU Scattering Analysis Interactive Dialin Nucleon-Nucleon Program (unpublished); private communication; R. A. Arndt *et al.*, Phys. Rev. D **28**, 97 (1983); **35**, 128 (1987).
[52] J. Raynal, computer code, ECIS, 1979 (unpublished).
[53] G. J. Pyle, computer code RAROMP, University of Minnesota, Informal Report, C00-1265-64, 1964 (unpublished), modified for relativistic energies.
[54] See, for example, A. Bohr and B. Mottelson, *Nuclear Structure* (Benjamin, Reading, MA, 1975), Vol. II, Chap. 6.
[55] D. D. Warner and R. F. Casten, Phys. Rev. Lett. **48**, 1385 (1982); Phys. Rev. C **28**, 1798 (1983).
[56] O. Scholten, F. Iachello, and A. Arima, Ann. Phys. (N.Y.) **115**, 325 (1978).
[57] O. Scholten, Kernfisisch Versneller Instituut Internal Report No. 63, 1979.
[58] A. Arima, T. Otsuka, F. Iachello, and I. Talmi, Phys. Lett. **66B**, 205 (1977).
[59] T. Otsuka, A. Arima, F. Iachello, and I. Talmi, Phys. Lett. **76B**, 139 (1978).
[60] R. Bijker, A. E. L. Dieperink, O. Scholten, and R. Spanhoff, Nucl. Phys. **A344**, 207 (1980).
[61] H. C. Chiang, S. T. Hsieh, M. M. K. Yen, and C. S. Han, Nucl. Phys. **A435**, 54 (1985).
[62] G. L. Long, Y. X. Liu, and H. Z. Sun, J. Phys. G **16**, 813 (1990).
[63] K. A. Sage and B. R. Barrett, Phys. Rev. C **22**, 1765 (1980).
[64] R. D. R. Raju, Phys. Rev. C **23**, 518 (1981).
[65] P. B. Goldhoorn, M. N. Harakeh, Y. Iwasaki, L. W. Put, F. Zwartz, and P. Van Isacker, Phys. Lett. **103B**, 291 (1981).
[66] K. A. Sage, P. R. Goode, and B. R. Barrett, Phys. Rev. C **26**, 668 (1982).
[67] P. Van Isacker, K. Heyde, M. Waroquier, and G. Wenes, Phys. Lett. **104B**, 5 (1981); Nucl. Phys. **A380**, 383 (1982).
[68] K. Heyde, P. Van Isacker, M. Waroquier, G. Wenes, Y. Gigase, and J. Stachel, Nucl. Phys. **A398**, 235 (1983).
[69] J. Dukelsky, J. F. Niello, H. M. Sofia, and R. P. Perazzo, Phys. Rev. C **28**, 2183 (1983); J. Dukelsky, G. G. Dussel, and H. M. Sofia, Phys. Lett. **100B**, 367 (1981).
[70] H. C. Wu and X. Q. Zhou, Nucl. Phys. **A417**, 67 (1984).
[71] F. Todd Baker, Phys. Rev. C **32**, 1430 (1985).
[72] N. Yoshinaga, Y. Akiyama, and A. Arima, Phys. Rev. Lett. **56**, 1116 (1986); T. Otsuka, A. Arima, and N. Yoshinaga, *ibid.* **48**, 387 (1982).
[73] Y. Akiyama, Nucl. Phys. **A433**, 369 (1986).
[74] S. Kuyucak and I. Morrison, Phys. Rev. Lett. **58**, 315 (1987); Phys. Lett. B **255**, 305 (1991).
[75] Y. D. Devi and V. K. B. Kota, Z. Phys. A **337**, 15 (1990).
[76] I. Morrison, J. Phys. G **12**, L201 (1986).
[77] W. Boeglin, P. Egelhof, I. Sick, J. M. Cavedon, B. Frois, D. Goutte, V. Meot, P. Leconte, X. H. Phan, S. K. Platchkov, S. Williamson, and M. Girod, Nucl. Phys. **A477**, 399 (1988).